

Article

**Sum Frequency Generation Imaging Microscopy of  
Patterned Self-Assembled Monolayers with Terminal #CH,  
#OCH, #CF<sub>2</sub>, #C#C, #Phenyl, and #Cyclopropyl Groups**

Katherine Cimatu, H. Justin Moore, David Barriet,  
Pawilai Chinwangso, T. Randall Lee, and Steven Baldelli

*J. Phys. Chem. C*, **2008**, 112 (37), 14529-14537 • DOI: 10.1021/jp804707w • Publication Date (Web): 20 August 2008

Downloaded from <http://pubs.acs.org> on April 15, 2009

**More About This Article**

Additional resources and features associated with this article are available within the HTML version:

- Supporting Information
- Links to the 1 articles that cite this article, as of the time of this article download
- Access to high resolution figures
- Links to articles and content related to this article
- Copyright permission to reproduce figures and/or text from this article

[View the Full Text HTML](#)

# Sum Frequency Generation Imaging Microscopy of Patterned Self-Assembled Monolayers with Terminal $-\text{CH}_3$ , $-\text{OCH}_3$ , $-\text{CF}_2\text{CF}_3$ , $-\text{C}=\text{C}$ , $-\text{Phenyl}$ , and $-\text{Cyclopropyl}$ Groups

Katherine Cimatu, H. Justin Moore, David Barriet, Pawilai Chinwangso, T. Randall Lee,\* and Steven Baldelli\*

Department of Chemistry, University of Houston, Houston, Texas 77204-5003

Received: May 28, 2008; Revised Manuscript Received: July 3, 2008

Vibrational spectroscopic imaging is demonstrated for a variety of organic monolayer-functionalized surfaces patterned using microcontact printing. The images from sum frequency generation imaging microscopy (SFGIM) are analyzed using different contrast mechanisms in the interpretation of the transition from stamped to backfilled regions of interest. For this experiment, microcontact printing is used to spatially control the surface monolayers by using a patterned stamp and by varying the terminal functional group of the backfilling solutions. Analysis by the three different methods suggests that significant mixing occurs between the stamped and backfilled regions, which influence the contrast in the images at the resonant peaks. In addition, the interference between the resonant peaks and nonresonant background also has an effect on the appearance of the image.

## Introduction

For the past several years, soft lithography or microcontact printing ( $\mu\text{CP}$ ) has drawn significant interest, ranging from studies of the formation of monolayers to the use of patterned monolayers in various applications in microelectronics and medical diagnostics.<sup>1–6</sup> The advantages of using this method include simultaneous spatial and chemical control over the composition of the surface. The formation and modification of patterns on a surface is convenient through self-assembled monolayers (SAMs) and allows the observation of chemical contrast over the regions of interest (ROIs), allowing them to be studied independently.<sup>6,7</sup> With this motivation, several microscopic and spectroscopic techniques have been used to study the processes involved in pattern formation. All of these significant approaches have both advantages and limitations. For example, atomic force microscopy (AFM) provides excellent spatial resolution; however, it lacks specific chemical information regarding the composition of the surface. On the other hand, chemical force microscopy, one of its derivatives, provides contrast based on surface functionality in relation to friction/adhesion properties.<sup>8,9</sup> Furthermore, X-ray techniques, such as X-ray photoemission electron microscopy (XPEEM) and near-edge X-ray absorption fine structure (NEXAFS), where both were used for providing contrast with good spatial resolution in lithographic samples.<sup>10–12</sup> Although several spectroscopic techniques, such as Fourier transform infrared (FTIR) microscopy, have been used to provide chemical information of the molecules present on the surface, these techniques lack interface specificity. Consequently, for the characterization of electrodes and various catalytic surfaces, the attempted use of FTIR spectroscopic/microscopic techniques to collect monolayer-specific information is typically convoluted with or overwhelmed by signals from the contacting bulk solution.<sup>13</sup>

Thus, to overcome these limitations, sum frequency generation imaging microscopy (SFGIM) has been developed.<sup>14–17</sup> Sum frequency generation (SFG) spectroscopy is a vibrational spectroscopic technique that is interface specific, providing

chemical information of molecules near a surface. Kuhnke and co-workers were able to chemically and spatially identify the molecules on a surface, where the contrast was related to the vibrational properties of the molecules.<sup>14–16</sup> For the interpretation of SFG images, they used electronic and vibrational contrast mechanisms to obtain the molecular coverage on the surface. Their analysis showed that the signal intensity varied with the wavenumber. To obtain the coverage of the molecules at each location, they subtracted the nonresonant background from the resonant intensity divided by the average nonresonant intensity.

The previous results using SFGIM to characterize the patterned  $\mu\text{CP}$  SAMs on gold<sup>17–20</sup> detected a change in contrast that was predominantly dependent on the inherent vibrational properties/spectrum of the molecules on the surface. This interpretation was successful in the analysis of several monolayer systems, such as SAMs in  $\mu\text{CP}$ , carbon monoxide on platinum, probing heterogeneous surfaces such as octadecanethiol (ODT) on mild steel, and exploring the variation in monolayer structure across the surface of zinc.<sup>17–21</sup>

The goal of the present work is to study the physical, chemical, and spectroscopic parameters that influence the contrast and chemical resolution in nonlinear vibrational spectroscopic imaging (i.e., SFGIM) and to develop a more detailed model of the mixing of adsorbates in  $\mu\text{CP}$  SAMs. The contrast depends on the nature of the molecules (resonant factor), how the molecules are assembled on the substrate, chain-length, number of sulfur atoms attached to the metal substrate, exchange between stamped (adsorbed) molecules and the molecules in the backfilling solution, and the lateral diffusion between stamped and backfilled molecules. The contrast is also dependent on optical factors such as beam profile for 1064 nm and infrared beams, metal substrate (nonresonant background), preparation, and purity of gold.

$\mu\text{CP}$  was used with different  $\omega$ -functionalized alkanethiols to spatially and chemically modify the surface of the sample. Chemical modification provides distinct vibrational spectra, which provides visual contrast when the IR beam is in resonance with the molecules, regardless of the nature of the metal substrate. However, because of its electronic nature, the gold

\* Corresponding author.

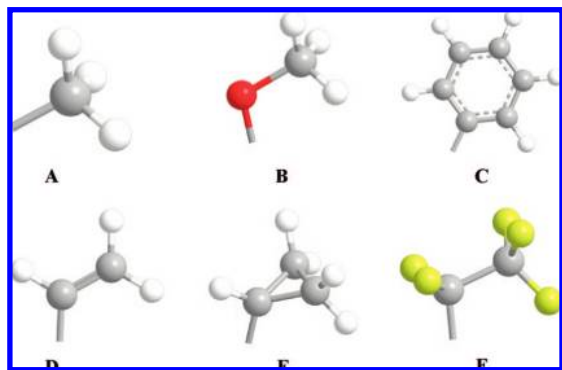


**Figure 1.** Structure of the molecules used to vary the chemical functionality and vibrational contrast in SFGIM. (A) hexadecanedithiocarboxylic acid, (B) 16-methoxyhexadecanethiol, (C) 16-phenylhexadecanethiol, (D) 17-octadecenethiol, (E) 16-cyclopropylhexadecanethiol, and (F) 15,15,16,16,16-pentafluorohexadecanethiol.

substrate exhibits a high nonresonant signal with a phase opposite to that of the adsorbates;<sup>22</sup> consequently, the SFG spectrum displays dips instead of peaks when the molecules are in resonance. As a result of its strong intensity, the signal from gold serves as a baseline and gives rise to an interference effect between the molecules and the substrate; on resonance regions where the molecules reside, the regions appear dark in the image.

The information obtained from these experiments and presented in this paper can be used to interpret contrast in the images. We anticipated that each of the molecules tested would have varying vibrational contrast and interpretation; as such, three methods were used to interpret the contrast in the SFG images of  $\mu$ CP monolayers. In all experiments, hexadecanedithiocarboxylic acid (A in Figure 1) was used as the stamped molecule. Previous studies have shown that this adsorbate undergoes little exchange/diffusion and provides good edge contrast.<sup>19</sup> We then varied the backfilling solution used in each experiment by employing the following alkanethiols, which possess distinct terminal groups: (B) 14-methoxytetradecanethiol, (C) 16-phenylhexadecanethiol, (D) 17-octadecenethiol, (E) 16-cyclopropylhexadecanethiol, and (F) 15,15,16,16,16-pentafluorohexadecanethiol (see Figure 1).

**SFG Theory.** Although SFG theory has been well reviewed, a few significant properties are summarized here since they are important to the interpretation of the SFG images. SFG is a second-order nonlinear process that is used to probe molecules at the interface between two media. The technique involves the overlap of two pulsed laser beams at the surface, generating a third beam with a frequency that is the sum of the two input frequencies. The SFG intensity,  $I_{\text{SF}}$ , is defined as follows:

$$I_{\text{SF}} \propto \left| \sum_{\text{JK}} \chi_{\text{IJK}}^{(2)} E_{\text{J}}(\omega_{\text{vis}}) E_{\text{K}}(\omega_{\text{IR}}) \right|^2 \quad (1)$$

where  $\chi_{\text{IJK}}^{(2)}$  is the second-order nonlinear surface susceptibility, and the  $E(\omega)$  terms are light field amplitudes. The susceptibility tensor,  $\chi_{\text{IJK}}^{(2)}$ , contains the information of the molecules at the interface. The resonant portion contains the vibrational information of the molecules,  $\chi_{\text{R}}^{(2)}$ , while the nonresonant susceptibility is primarily due to the gold substrate,  $\chi_{\text{NR}}^{(2)}$ :

$$\chi^{(2)} = \chi_{\text{R}}^{(2)} + \chi_{\text{NR}}^{(2)} = \sum_q \frac{A_q}{\omega_{\text{IR}} - \omega_q + i\Gamma} + \chi_{\text{NR}}^{(2)} \quad (2)$$

where  $\omega_{\text{IR}}$  and  $\omega_q$  are the infrared frequency and the resonant frequency of the  $q$ th vibrational mode, respectively. The

damping factor of the vibration is  $\Gamma$ . The  $A_q$  term contains information regarding infrared and Raman transition moments.

Since SFG at the interface is the combination of both resonant and nonresonant signals,  $\chi^{(2)} = \chi_{\text{R}}^{(2)} + \chi_{\text{NR}}^{(2)}$ , which are complex quantities, the total SFG signal greatly depends on the relative phases,  $\varepsilon$  and  $\delta(\omega_{\text{IR}})$ , of the two susceptibilities. In polar coordinates, susceptibilities are described with magnitude and phase. Therefore, the overall susceptibility is shown as the summation of both:<sup>22,23</sup>

$$\chi_{ijk}^{(2)} = |\chi_{\text{R}}^{(2)}| e^{i\delta(\omega_{\text{IR}})} + |\chi_{\text{NR}}^{(2)}| e^{i\varepsilon} \quad (3)$$

$\delta(\omega_{\text{IR}})$  is the resonant phase, which depends on the IR frequency. The symbol  $\varepsilon$  is referred to as the fixed nonresonant phase, which is approximately invariant with IR frequency and dependent on the intrinsic properties of the metal.<sup>22</sup> The emitted SF light intensity from the interface is

$$I_{\text{SF}} \propto |\chi_{\text{R},ijk}^{(2)}|^2 + |\chi_{\text{NR},ijk}^{(2)}|^2 + 2|\chi_{\text{R},ijk}^{(2)}||\chi_{\text{NR},ijk}^{(2)}|\cos(\varepsilon - \delta(\omega_{\text{IR}})) \quad (4)$$

The magnitudes for the first two terms of susceptibilities are positive, and the cross-term might have a positive or a negative value. A positive cross-term forms constructive interference, thus giving rise to a peak. On the other hand, a negative cross-term forms a destructive interference, thus giving rise to a dip. Therefore, the relative phase difference in the cross-term between the two susceptibilities gives rise to peaks or semi-interference peaks. The resonant derivative line shapes also depend on the properties of the metal substrate and the polar orientation of the molecules at the interface.<sup>24–33</sup> Similarly, there is interference between adjacent peaks that can lead to an apparently complicated spectrum.

## Experimental Section

**Materials.** As shown in Figure 1, the following organosulfur compounds were used to prepare SAMs on gold: hexadecanedithiocarboxylic acid,<sup>34</sup> 14-methoxytetradecanethiol,<sup>35</sup> 16-phenylhexadecanethiol,<sup>36</sup> 16-cyclopropylhexadecanethiol,<sup>37</sup> and 15,15,16,16,16-pentafluorohexadecanethiol.<sup>38</sup> These molecules were synthesized using the procedures given in the indicated references.<sup>33–37</sup> Details regarding the synthesis and characterization of 17-octadecenethiol are provided as Supporting Information.

**Preparation of Gold Substrates.** The Si(100) wafers were attached to the rotating plate and cleaned with absolute ethanol before placing the wafers inside the bell jar of the evaporator. The evaporator was then evacuated for one hour to reach a pressure of  $1 \times 10^{-5}$  Torr. Once the targeted pressure was reached, the wafers were precoated with a 10 nm thick layer of chromium to promote the adhesion of gold to the silicon wafer. After this process, the gold substrates were prepared by evaporating 100 nm of gold onto the Si(100) wafers. The evaporator was left to cool for one hour and 30 min, and then the bell jar was opened. Once the gold films were removed from the evaporator, the quality of the film was evaluated by using ellipsometry.<sup>34,36,39</sup>

**Preparation of Polydimethylsiloxane (PDMS) Stamps.** The master pattern, which contains a series of 100, 20, 5, 2, 1, 8, and 50  $\mu\text{m}$  line patterns, was rinsed with methanol and dried in an oven. On the basis of established procedures,<sup>7,40</sup> the PDMS stamp was prepared by mixing a 10:1 ratio of SYLGARD 184 (prepolymer)<sup>2</sup> and the curing agent in a clean, dry beaker. The prepolymer was stirred for 5 min and poured onto the master pattern. The prepolymer was then left untouched for approximately 15 min to reduce the air bubbles present in the mixture. After 15 min, the Petri dish containing the master

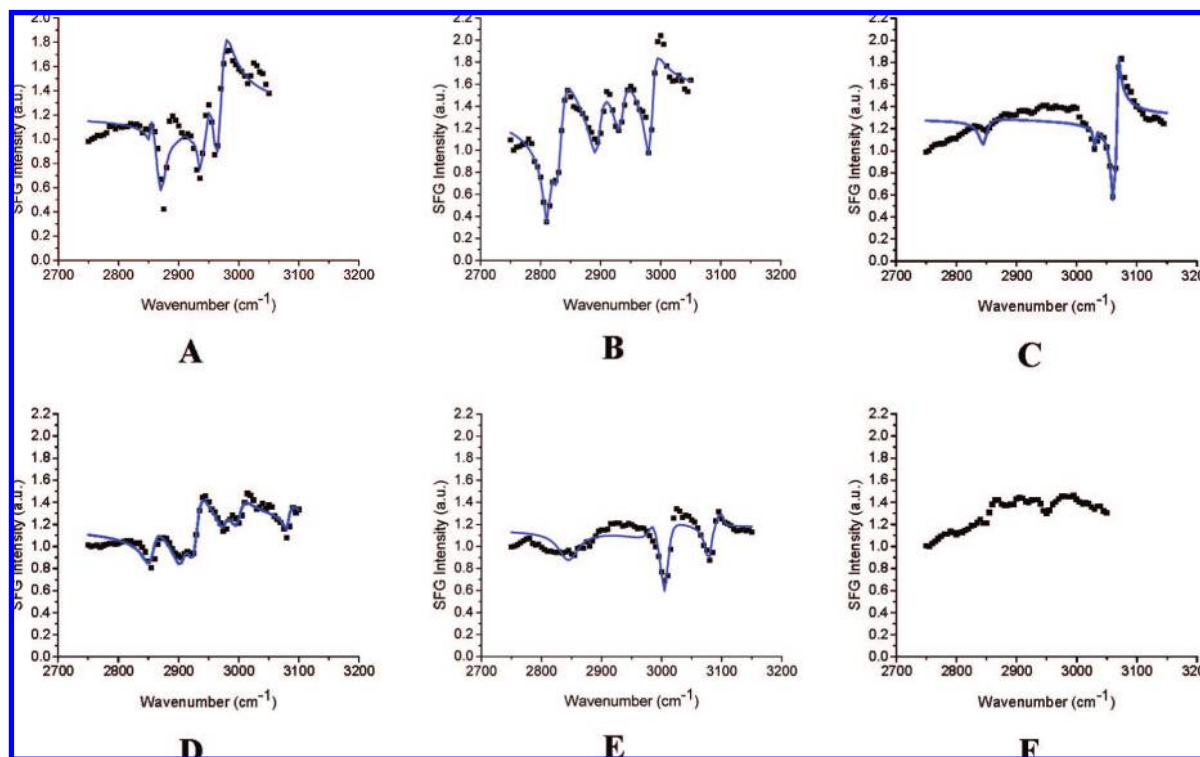


**Figure 2.** Average spectra of the adsorbates on gold prepared in solution. (A) hexadecanedithiocarboxylic acid, (B) 16-methoxyhexadecanethiol, (C) 16-phenylhexadecanethiol, (D) 17-octadecanethiol, (E) 16-cyclopropylhexadecanethiol, and (F) 15,15,16,16,16-pentafluorohexadecanethiol. Lines are curve-fitted using eq 2.

pattern and the prepolymer was placed inside the drying oven at slightly elevated temperature (40–45 °C) overnight. After complete polymerization, the PDMS polymer/stamp was removed from the oven and cooled to room temperature. The specific pattern on the mold was slowly removed by tweezers. After removing the mold, the stamp was rinsed and sonicated in ethanol for 5 min, placed in a clean beaker, and dried in an oven.<sup>1</sup>

**Preparation of Stamped Samples.** Four drops of the 1 mM dithiolcarboxylic acid solution were placed upon the surface of the PDMS stamp containing the pattern. The stamp was then dried with nitrogen gas. The face of the stamp containing the line features was carefully stamped for 15 min, without weight, onto the gold surface. After printing, the stamp was gently removed, and the gold surface was rinsed with ethanol to remove any unattached hexadecanedithiocarboxylic acid molecules and dried under a stream of nitrogen gas. The patterned gold substrates for each independent experiment were placed for 5 min into the 1 mM ethanolic solutions containing the respective backfilling molecules.

**Laser, SFGIM, and SFG Details.** A picosecond pulsed Nd:YAG laser (from EKSPILA) was used in the  $\mu$ CP experiments. The Nd:YAG laser generated a 1064 nm beam that pumped the optical parametric generator/amplifier (OPG/OPA) to generate a tunable IR beam (2000–4000  $\text{cm}^{-1}$ ). Both the 1064 nm and IR beams were used in probing the surface to generate the SFG beam for the microscope setup.<sup>28</sup>

The beams, set to p-polarization, were overlapped at the interface at 70.0° and 60.0° from the surface normal at exactly the same time and place. In this configuration, the output SFG occurs at 62.1°. A short-pass filter was placed after the sample position to attenuate/block the 1064 nm reflection. A telescope consisting of a combined lens system was positioned after the filter to maintain the 1:1 image ratio onto the grating, which diffracted the beam perpendicular to the 10X objective that

magnifies the intermediate image onto a Roper 1024  $\times$  1024 pixel array CCD camera.

**Data Collection and Image Processing.** Images and spectra were acquired by tuning the IR frequency at a fixed scan rate and averaging the SFG signal over an interval of 5  $\text{cm}^{-1}$ . The images obtained were background corrected with the IR blocked for the same number of accumulations (5000) for each image. No other image processing was performed on the images. After acquisition, the images were stacked according to increasing wavenumber (for every 5  $\text{cm}^{-1}$ ) using an Image J program.<sup>41</sup> The spectral range for each experiment depends on the functional group of the backfilling molecule. The spectral data were obtained using the same program by choosing and averaging a specific number of pixels in a given ROI (depending on which size is chosen to obtain the data). The results were plotted using Origin software. The ROIs for the data acquisitions presented are specified in the Results section.

The scale bar of 150  $\mu\text{m}$  presented in Figure 3B is the same for all the SFG images presented in the figures.

## Results

**SFG Reference Spectra.** The spectra shown in Figure 2 are representative of SAMs with various terminal functional groups deposited from solution on smooth gold surfaces. These spectra serve as the baseline to interpret the SFG images since the organosulfur molecules are without contamination and invariant with regard to spatial location (within SFGIM resolution). Further, all spectra were taken using the SFG microscope to ensure no differences arise from the experimental apparatus. Most resonances occur as dips in the spectra against the nonresonant background of gold. Table 1 provides a list of the spectral bands/IR wavenumber positions with their respective vibrational assignments.

**SFG Images of Various Functional Groups.** The images and spectra presented in Figures 3–7 demonstrate the range of

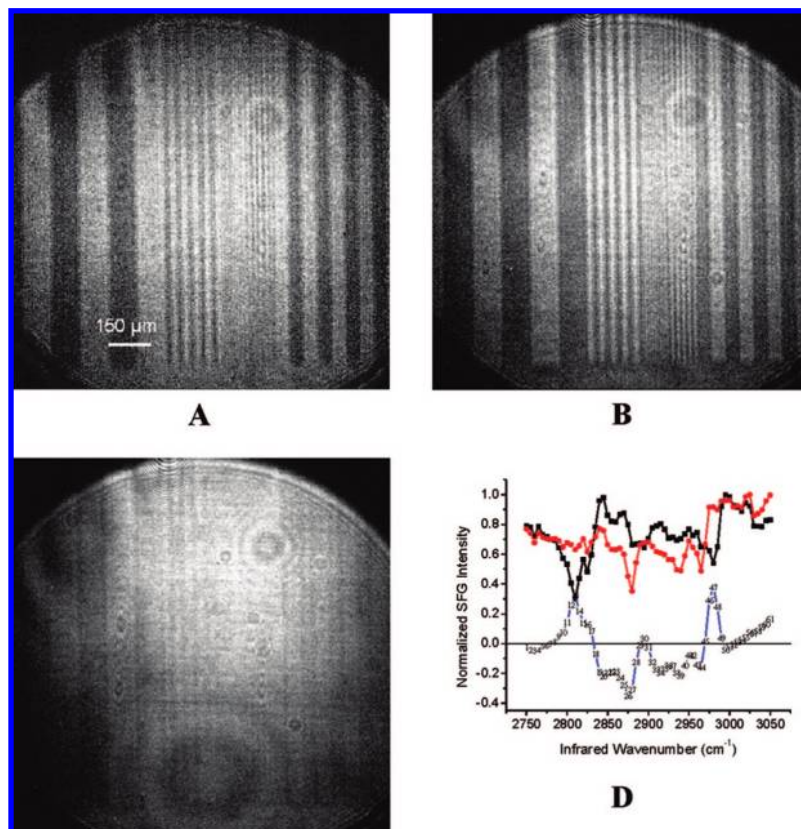


**Figure 3.**  $\mu$ CP hexadecanedithiocarboxylic acid backfilled with 16-methoxyhexadecanethiol, where the images were taken at (A) 2810  $\text{cm}^{-1}$ , (B) 2875  $\text{cm}^{-1}$ , and (C) 3000  $\text{cm}^{-1}$ . Spectra were acquired over an area of 100  $\mu\text{m}^2$  for (D) backfilled 16-methoxyhexadecanethiol, stamped hexadecanedithiocarboxylic acid region, and the difference of the two regions (stamped – backfilled) normalized to the intensity at 2755  $\text{cm}^{-1}$ .

**TABLE 1: List of Vibrational Assignments of the Resonances Observed in the Respective Vibrational Spectrum of Each Individual Adsorbate on Au (Solution-Deposited from 1 mM Solution in Ethanol)**

compound	wavenumber ( $\text{cm}^{-1}$ )	vibrational assignment
hexadecanedithiocarboxylic acid <sup>34,39</sup>	2850	methylene ( $\text{CH}_2$ ) symmetric stretch <sup>42–45</sup>
	2875	methyl ( $\text{CH}_3$ ) symmetric stretch <sup>42–45</sup>
	2915	methylene ( $\text{CH}_2$ ) antisymmetric stretch <sup>42–45</sup>
	2935	Fermi resonance of the methyl ( $\text{CH}_3$ ) symmetric stretch <sup>42–45</sup>
	2965	methyl ( $\text{CH}_3$ ) antisymmetric stretch <sup>42–45</sup>
14-methoxytetradecanethiol <sup>46</sup>	2810	A' out-of-plane $\text{OCH}_3$ stretch, doublet <sup>45,46</sup>
	2830	A' out-of-plane $\text{OCH}_3$ stretch, doublet <sup>45,46</sup>
	2895	overtone of antisymmetric $\text{CH}_3$ methyl deformation mode <sup>45,46</sup>
	2930	A'' out-of-plane $\text{CH}_3$ stretch <sup>45,46</sup>
	2980	$\text{CH}$ in-plane stretch mode, single <sup>45,46</sup> ( $\text{CH}_3$ )
16-phenylhexadecanethiol	3035	aromatic $\text{CH}$ stretch mode of the phenyl ring <sup>45</sup>
17-octadecanethiol	3065	
	2855	methylene ( $\text{CH}_2$ ) symmetric stretch <sup>42–45</sup>
	2905	methylene ( $\text{CH}_2$ ) antisymmetric stretch <sup>42–45</sup>
	2929	unassigned
	2975	unassigned
	3000	$\text{CH}$ stretch, $\text{CH}_2$ symmetric stretch $=\text{CH}_2$ <sup>45</sup>
	3083	$\text{CH}_2$ antisymmetric stretch $=\text{CH}_2$ <sup>45</sup>
16-cyclopropylhexadecanethiol	3005	$\text{CH}$ stretch, $\text{CH}_2$ symmetric stretch <sup>45</sup>
	3083	$\text{CH}_2$ antisymmetric stretch <sup>45</sup>
15,15,16,16-pentafluorohexadecanethiol <sup>47</sup>	2950	unassigned

molecules and chemical functionality that have been imaged with SFGIM. Functional groups such as methyl, methoxy, phenyl, pentafluoroethyl, vinyl, and cyclopropyl show contrast in the  $\mu$ CP patterns at specific vibrational frequencies compared to the stamped region of the methyl-terminated SAM derived from hexadecanedithiocarboxylic acid. Qualitatively, the images all show contrast, indicating that a pattern was formed; however, local spectra must be examined to assess the chemical purity of the stamped and backfilled regions. This topic is considered later in the paper.

## Discussion

**SFGIM Interpretation I.** The contrast in Figures 3–7 (with Figures 3 and 4 as examples) can be interpreted in the following manner: to a first approximation, the dark areas in the image are related to the resonance peaks in the SAMs. Thus, if the SFG spectra of the pure SAMs are known, or acquired independently, the intensity of the patterns can be predicted. This process is illustrated from the difference SFG spectra shown in Figure 3D and 4D. The spectra are both normalized to an

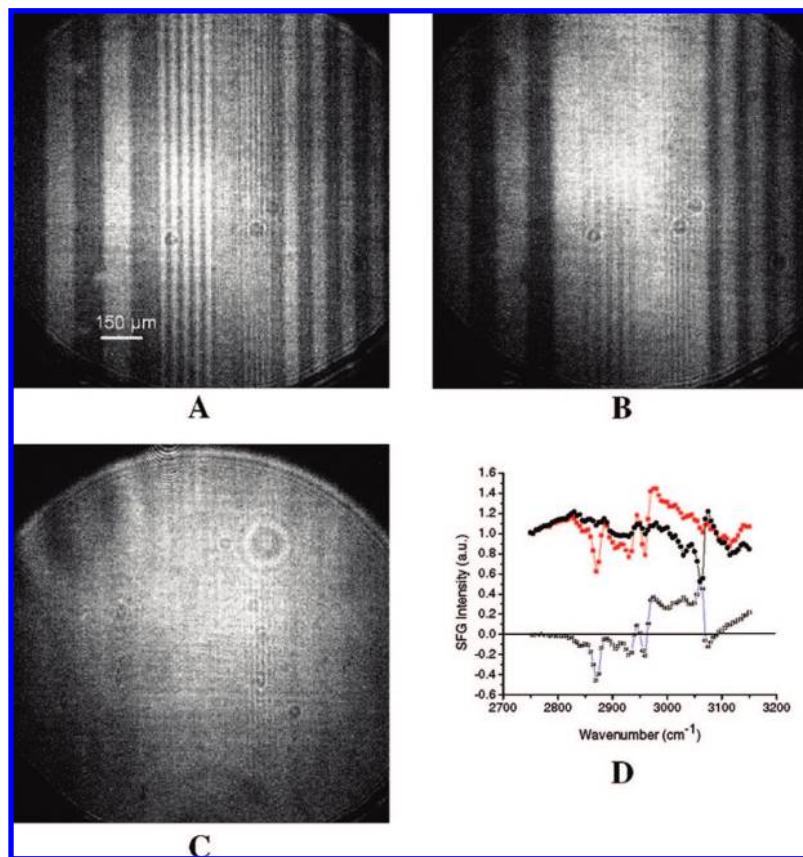


**Figure 4.**  $\mu$ CP hexadecanedithiocarboxylic acid backfilled with 16-phenylhexadecanethiol, where the images were taken at (A) 2875  $\text{cm}^{-1}$ , (B) 3065  $\text{cm}^{-1}$ , and (C) 2900  $\text{cm}^{-1}$ . Spectra were acquired over an area of 100  $\mu\text{m}^2$  for (D). Spectra obtained from the stack: the spectrum with the black square symbols is from the phenyl-terminated backfilled region collected from 2750–3150  $\text{cm}^{-1}$ ; the spectrum with the blue circle symbols is from the stamped region, and the spectrum with numeric symbols is the difference spectrum of the stamped and backfilled regions (stamped – backfilled).

off-resonance part of the spectrum at 2755  $\text{cm}^{-1}$ . Next, the difference between the spectra is taken, (stamped – backfilled) region. To interpret the image at a certain point on the surface, consider Figure 3D, where the plot shows that there is a difference in signal when a deviation occurs from zero. The image becomes dark whether it is on a methoxy-terminated or methyl-terminated region of the surface. If the signal becomes negative, then it corresponds to the methyl-terminated region; but, on the other hand, if the signal is positive, then it corresponds to the methoxy-terminated region. (Note: the image becomes dark for both peaks, whether positive or negative.) Thus, the positive signals at 2820  $\text{cm}^{-1}$  and 2980  $\text{cm}^{-1}$  correspond to the methoxy surface. Similarly, the negative signals at 2875  $\text{cm}^{-1}$ , 2935  $\text{cm}^{-1}$ , and 2955  $\text{cm}^{-1}$  correspond to the methyl-terminated surface. In addition, this same analysis is shown for the phenyl-terminated SAMs as the backfilling molecule in Figure 4. This contrast analysis demonstrates only one of the methods for the interpretation of the SFG images. Another strategy for contrast in SFGIM is the use of spectral-dependent line scans (cross sections), as shown in Figure 8, where the images are obtained at various wavenumbers as indicated. At positions where the IR is resonant with the SAM, the image becomes dark, since the vibrational resonances are dips in the SFG spectra against a bright signal from gold. Thus, the image contrast inverts from methyl-terminated SAMs (2875  $\text{cm}^{-1}$ ) to methoxy-terminated SAMs ( $\sim$ 2810  $\text{cm}^{-1}$ ) as well as at other wavenumbers. The image contrast approaches a minimum at the isosbestic points indicated in Figure 10 (i.e., 2895  $\text{cm}^{-1}$ ). Similarly, this effect is observed in the line scans of the pattern at various infrared wavenumbers. The images are

shown at various resonant and nonresonant portions of the spectra with the corresponding line scan displayed above the image. In these line scans, as the resonance factor becomes stronger, the image contrast increases, and the resolution of the features also increases. The cross sections show how the total intensity across the image changes. For example, in the nonresonant position of 2750  $\text{cm}^{-1}$ , Figure 8A shows little image contrast, and its the line profile has a Gaussian-like shape, where the shape and the beam profile are due to the nonresonant signal of gold. However, as the IR is tuned into resonance (vibrational modes of the molecules at the surface), for example at 2875  $\text{cm}^{-1}$ , the contrast in the images and step features in the line scan appear sharp (see Figure 8B). The line scans shown in Figure 8D are the result of subtracting the 2815  $\text{cm}^{-1}$  line scan from the 2755  $\text{cm}^{-1}$  line scan, thus minimizing the effect of the nonresonant gold signal/beam profile on the analysis. Also shown in Figure 8D is a zoomed-in line scan that displays the limiting spatial resolution of  $\sim$ 2  $\mu\text{m}$ . The contrast minimum predicted by the simulation in Figure 10 is only approximated when compared to the images in Figure 8, since these images are obtained over a 5  $\text{cm}^{-1}$  range and the simulation is at a single wavelength (discussed below).

**SFGIM Interpretation II, Chemical Maps.** Figure 9 shows SFG images where the signal from the methoxy-terminated SAM is color-coded red, and the signal from the methyl-terminated SAM is color-coded green. The images in Figure 9C,D show the regions of the two SAMs in one image, where panels A and B have been merged together to create the chemical map of the respective SAMs. The difference between panel C and panel D is that panel C represents the integrated

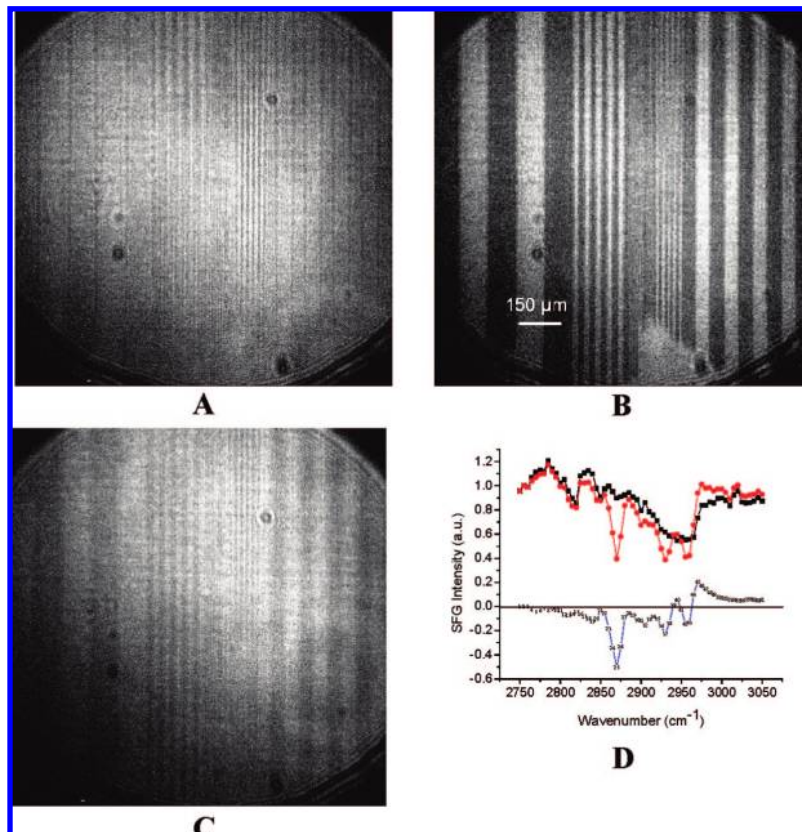


**Figure 5.**  $\mu$ CP hexadecanedithiocarboxylic acid backfilled with 15,15,16,16,16-pentafluorohexadecanethiol, where the images were taken at (A) 2855  $\text{cm}^{-1}$ , (B) 2870  $\text{cm}^{-1}$ , and (C) 2945  $\text{cm}^{-1}$ . (D) Backfilled 16,15,15,16,16,16-pentafluorohexadecanethiol, stamped hexadecanedithiocarboxylic acid region, and the difference of the two regions (stamped – backfilled) normalized to the intensity at 2755  $\text{cm}^{-1}$ .

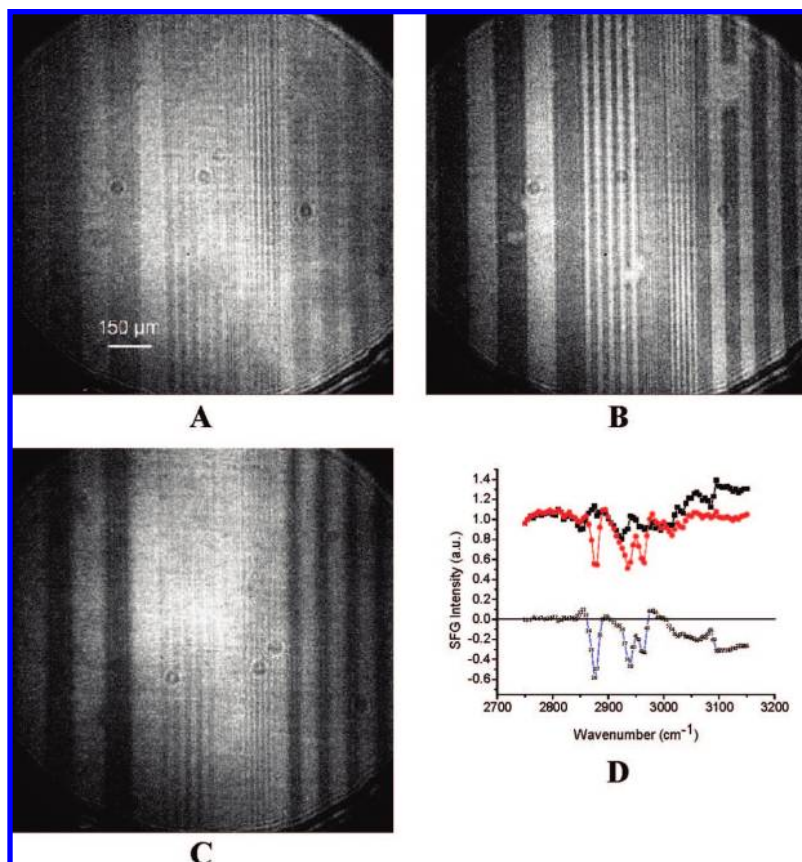


**Figure 6.**  $\mu$ CP hexadecanedithiocarboxylic acid backfilled with 17-octadecenethiol, where the images were taken at (A) 2850  $\text{cm}^{-1}$ , (B) 2875  $\text{cm}^{-1}$ , and (C) 3080  $\text{cm}^{-1}$ . (D) Backfilled 17-octadecenethiol, stamped hexadecanedithiocarboxylic acid region, and the difference of the two regions (stamped – backfilled) normalized to the intensity at 2755  $\text{cm}^{-1}$ .

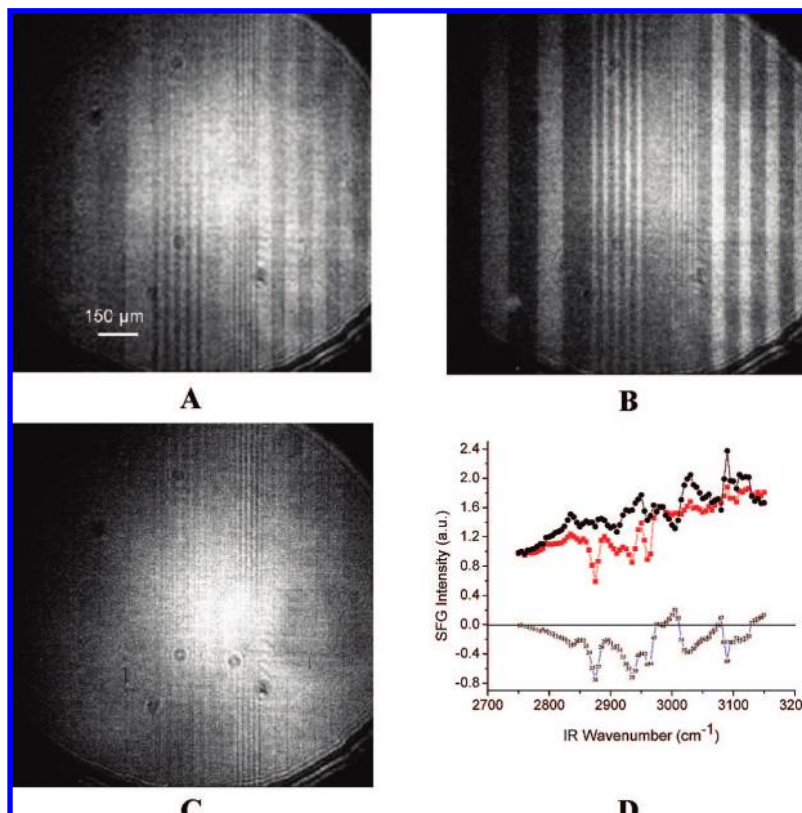


**Figure 7.**  $\mu$ CP hexadecanedithiocarboxylic acid backfilled with 16-cyclopropylhexadecanethiol, where the images were taken at (A)  $2800\text{ cm}^{-1}$ , (B)  $2875\text{ cm}^{-1}$ , and (C)  $3005\text{ cm}^{-1}$ . (D) Backfilled 16-cyclopropylhexadecanethiol, stamped hexadecanedithiocarboxylic acid region, and the difference of the two regions (stamped – backfilled) normalized to the intensity at  $2755\text{ cm}^{-1}$ .

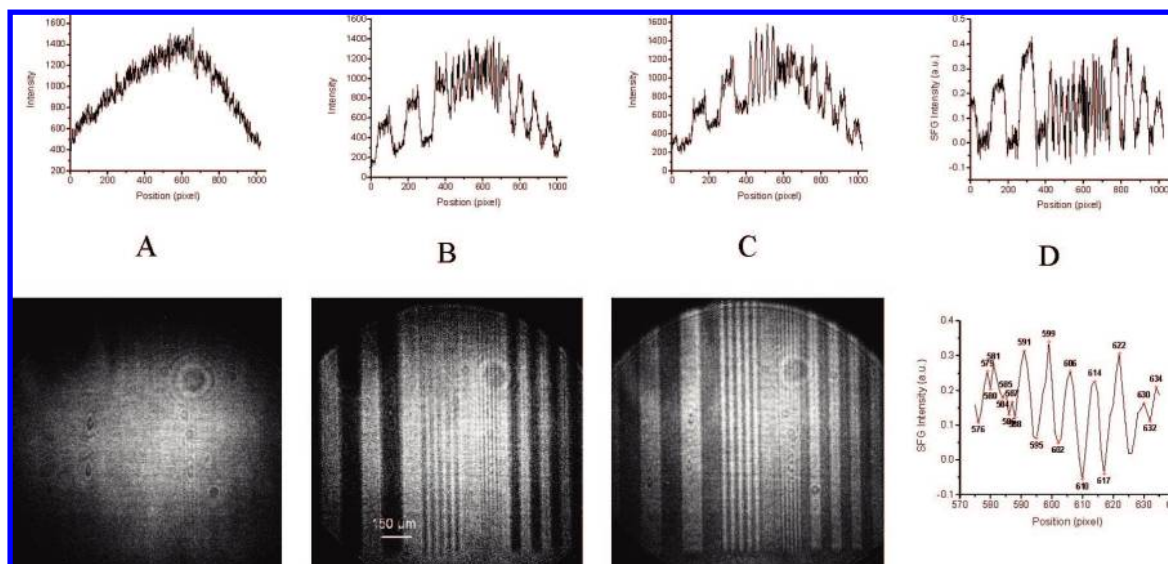


**Figure 8.** SFG images and line scan cross sections for the methyl-terminated stamped regions and the methoxy-terminated backfilled regions, at off-resonant wavenumber (A), resonant with methoxy-terminated (B), and resonant at methyl-terminated (C). Position refers to the number in the difference spectra of Figure 3F. (D) Line scans from the image at  $2815\text{ cm}^{-1}$ , corrected for the Gaussian laser profile. Peak labels indicate position in micrometers.

bands, while D represents a single wavelength (peak) image. The color scales of Figure 9A,B are inverted before they are merged, since the resonant peaks are dark in both images.

The images in Figure 9 can be related to the results presented in Figure 3D. The plots in Figure 3D show the results of taking the difference between the methoxy-terminated SAM and the methyl-terminated SAM. In the difference spectrum, the positive peaks indicate where the signal from the methoxy-group dominates, while the negative peaks indicate where the signal

from the methyl-group dominates. The color separation is nearly complete; however, the red + green region has some mixing and might appear yellow or as separate discrete colors, indicating mixing of the monolayers. In conclusion, bright and dark contrasts (grayscale) were useful to interpret the spectral features and resonant imaging of different functional groups; the color maps are useful to interpret the distribution of the different SAMs on the surface. As suggested by the images,  $\mu$ CP using dithiocarboxylic acid inks appears to be a relatively pure process,

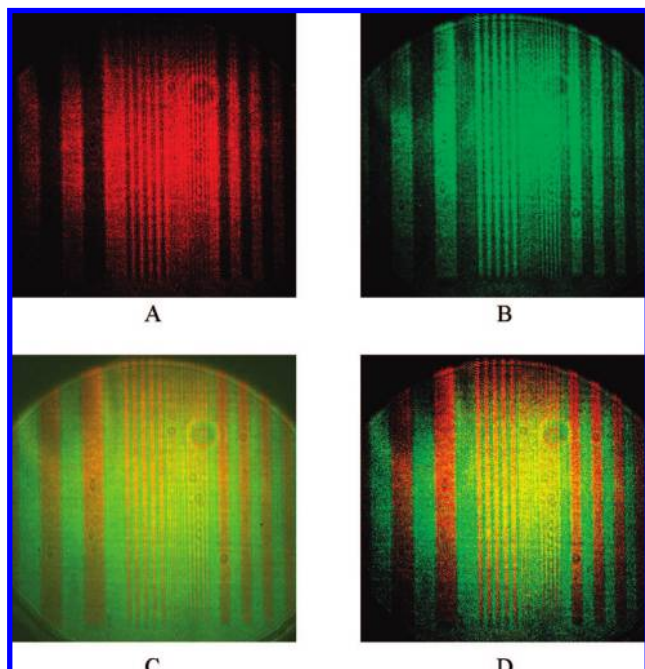


**Figure 9.** Color-coded SFG image of methoxy-terminated region (red), and methyl-terminated region (green). Single images: (A) color-scale red for methoxy-terminated SAM, and (B) color-scale green for methyl-terminated SAM. Merged images: (C) band integrated and (D) peak value.

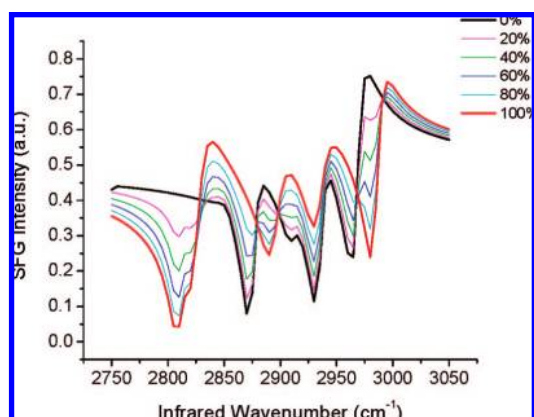


**Figure 10.** Simulation of methoxy-terminated and methyl-terminated SAMs. The legend refers to the percent of methoxy-terminated SAMs contributing to the SFG spectrum. The individual spectral properties are determined from the solution-deposited SAMs.

since there is clear color differentiation; in contrast, the actual spectral analysis indicates that some degree of mixing occurs between the stamped and backfilled regions. Importantly, the degree of mixing is less when dithiocarboxylic acids are used as the stamping ink than when normal alkanethiols are used as the stamping ink.<sup>19</sup>

**Simulation of Monolayer Mixing.** The spectra and mixing of the monolayers can be estimated by simulating the SFG spectra for both the  $\mu$ CP and backfilled molecules. Figure 10 shows such a simulation for solution-deposited methyl-terminated and methoxy-terminated SAMs. The SFG spectra of each molecule deposited from solution are curve-fitted to eq 2 to extract the frequency, width, and amplitude of each peak, giving  $\chi_{\text{eff}}^{(2)}(\text{methyl})$ , and  $\chi_{\text{eff}}^{(2)}(\text{methoxy})$ , where each  $\chi_{\text{eff}}^{(2)}$  represents the resonant contribution to the SFG spectra. The simulated spectra are thus

$$I_{\text{SF}} = |\chi_{\text{NR}}^{(2)} + (1 - n)\chi_{\text{eff}}^{(2)}(\text{methyl}) + n\chi_{\text{eff}}^{(2)}(\text{methoxy})|^2$$

where  $\chi_{\text{NR}}^{(2)}$  is the nonresonant susceptibility, and “ $n$ ” is the fraction of methoxy-terminated species contributing to the SFG signal. This approximation assumes that only concentration influences the SFG signal, not orientation changes, and that  $\chi_{\text{NR}}^{(2)}$  is the same in both  $\mu$ CP and solution-deposited films.

There are several interesting features in the simulation of the individual and mixed spectra. First, there are several peaks that are relatively isolated for each molecule, which can thus serve as good indicators of the species present; for example, the  $\text{CH}_3$  (sym) of the methyl ( $2875 \text{ cm}^{-1}$ ) and methoxy ( $\sim 2815 \text{ cm}^{-1}$ ) groups. Further, there are several isosbestic points in the simulation; these are points where the SFG signal remains constant as the composition changes when the IR is scanned. As shown in Figure 10, these points appear at  $2878$ ,  $2897$ ,  $2968$ , and  $2991 \text{ cm}^{-1}$ . Since these points show the same intensity for the two SAMs, they represent ideal reference points to normalize the SFG spectra and images. For example, if the SFG spectra of the methoxy portion and the methyl portion of the pattern are normalized to one of these isosbestic points, then the resulting contrast in the images should be maximized, because these points are where the chemical contrast is at a minimum. Then, it should be possible to use principal-component analysis to quantify the fraction of each molecule at different regions of the surface using appropriate assumptions.

The contrast in the images for the various terminal groups is relatively similar for all the molecules studied, although the spectral purity between the stamped and backfilled regions is not, which means that some of the phenyl-terminated SAMs are present in the stamped region as a dip positioned at  $3060 \text{ cm}^{-1}$ . For example, the contrast in the images provided by backfilling with the methoxy-terminated and phenyl-terminated SAMs are very clear; similarly, after the image analysis, the spectra obtained for the stamped and backfilled regions are also well-defined when compared to the solution-deposited SAMs (e.g., compare the spectra in Figure 2 B,C with those in Figures 3 and 4, respectively) because of their distinct fingerprint in the spectra as indicated in Table 1 for the vibrational assignments. While the SFG spectra extracted from the  $\mu$ CP patterns of the pentafluoro- and cyclopropyl-terminated SAMs are not as distinct as their solution-deposited films (e.g., compare the spectra in Figure 2 with those in Figures 3 and 4, respectively), the contrast in the images obtained is still quite good in terms of the bright-and dark contrast difference in the regions based on the line pattern provided by the PDMS stamp. The difference in the SFG images and spectra probably arises from a difference in the quality of the SAMs in the stamped- and solution-deposited SAMs (1) due to the short printing time (15 min), (2) because the  $\mu$ CP SAMs are probably less densely packed, and (3) lastly, due to the possibility of disulfides present in the backfilling solutions, which limits the formation of SAMs in a given amount of time and less ordered when compared to those derived from solution deposition (24 h adsorption).

**Mechanism of SFG Contrast.** Contrast in the SFG images of patterned surfaces arises from several factors:

1. Concentration of each molecule in the stamped and backfilled regions (influenced by the deposition process and/or mixing).
2. Differences in the SFG spectra of the two molecules.
3. Degree of orientational ordering.
4. Instrumental factors.
5.  $\mu$ CP process (influenced by the quality of both the stamp and the gold substrate).

These SFG images presented here offer a new paradigm for the ready determination of the degree of molecular heterogeneity of mixed surfaces (both patterned and unpatterned). This determination relies on the contribution of each independent spectrum to the composite obtained from SFGIM, offering a unique alternative to other imaging techniques, such as secondary ion mass spectroscopy (SIMS), X-ray photoelectron spectroscopy (XPS), and NEXAFS and also for comparison purposes.

## Conclusions

In this study, we explored the use of a variety of chemical functional groups in SFG imaging. Our base system consisted of methyl-terminated SAMs derived from the adsorption of hexadecanedithiocarboxylic acid on the surface of gold.  $\mu$ CP patterns of the base SAM were backfilled with various  $\omega$ -terminated alkanethiols and evaluated by SFGIM. The results demonstrated that SFG imaging not only provided a chemically specific view of the resulting pattern, but it also allowed a facile determination of the degree of chemical purity in the patterned domains. Overall, the results presented here show that SFGIM can now be visualized through several contrast mechanisms, where the dominant contribution is due to the vibrational resonance of the respective molecules.

**Acknowledgment.** S.B. and K.C. are appreciative of funding by the NSF (0650779) and Ekspla. T.R.L. is grateful for generous financial support from the Texas Center for Superconductivity and the Robert A. Welch Foundation (Grant E-1320).

**Supporting Information Available:** The synthesis and characterization of the alkene-terminated thiol 17-octadecanethiol. This material is available free of charge via the Internet at <http://pubs.acs.org>.

## References and Notes

- Delamarche, E.; Schmid, H.; Bietsch, A.; Larsen, N. B.; Rothuizen, H.; Michel, B.; Biebuyck, H. A. *J. Phys. Chem. B* **1998**, *102*, 3324.
- Love, J. C.; Estroff, L. A.; Kriebel, J. K.; Nuzzo, R. G.; Whitesides, G. M. *Chem. Rev.* **2005**, *105*, 1103.
- Larsen, N. B.; Biebuyck, H.; Delamarche, E.; Michel, B. *J. Am. Chem. Soc.* **1997**, *119*, 3017.
- Xia, Y.; Whitesides, G. M. *Langmuir* **1997**, *13*, 2059.
- Xia, Y.; Whitesides, G. M. *J. Am. Chem. Soc.* **1995**, *117*, 3274.
- Biebuyck, H. A.; Whitesides, G. M. *Langmuir* **1994**, *10*, 2790.
- Miller, J. S.; Bethencourt, M. I.; Hahn, M.; Lee, T. R.; West, J. L. *Biotechnol. Bioeng.* **2006**, *93*, 1060.
- Tamada, K.; Hara, M.; Sasabe, H.; Knoll, W. *Langmuir* **1997**, *13*.
- Zhou, Y.; Fan, H.; Fong, T.; Lopez, G. P. *Langmuir* **1998**, *14*, 660.
- Klauser, R.; Hong, L.-H.; Wang, S.-C.; Zharnikov, M.; Paul, A.; Golzhauser, A.; Terfort, A.; Chuang, T. J. *J. Phys. Chem. B* **2003**, *107*, 13133.
- Zharnikov, M.; Shaporenko, A.; Paul, A.; Golzhauser, A.; Scholl, A. *J. Phys. Chem. B* **2005**, *109*, 5168.

- Hu, W. S.; Tao, Y. T.; Hsu, Y. J.; Wei, D. H.; Wu, Y. S. *Langmuir* **2005**, *21*, 226.
- Iwasita, T.; Nart, F. C. *Surf. Sci.* **1997**, *55*, 271.
- Kuhnke, K.; Hoffman, D. M. P.; Wu, X. C.; Bittner, A. M.; Kern, K. *Appl. Phys.* **2003**, *83*, 1.
- Hoffman, D. M. P.; Kuhnke, K.; Kern, K. *Nonlinear Spec. Proc. SPIE* **2002**, *4812*, 82.
- Hoffman, D. M. P.; Kuhnke, K.; Kern, K. *Rev. Sci. Instrum.* **2002**, *73*, 3221.
- Cimatu, K.; Baldelli, S. *J. Phys. Chem. B* **2006**, 110.
- Cimatu, K.; Baldelli, S. *J. Am. Chem. Soc.* **2006**, *128*, 16016.
- Cimatu, K.; Baldelli, S. *J. Phys. Chem. C* **2007**, *111*, 11751.
- Cimatu, K.; Baldelli, S. *J. Phys. Chem. C* **2007**, *111*, 7137.
- Cimatu, K.; Baldelli, S. *J. Am. Chem. Soc.* **2008**, *130*, 8030.
- Bain, D. C. *J. Chem. Soc., Faraday Trans.* **1995**, *91*, 1281.
- Bain, C. D.; Whitesides, G. M. *J. Am. Chem. Soc.* **1989**, *111*, 7164.
- Hunt, J. H.; Guyot-Sionnest, P.; Shen, Y. R. *Chem. Phys. Lett.* **1987**, *133*, 189.
- Superfine, R.; Guyot-Sionnest, P.; Hunt, J. H.; Kao, C. T.; Shen, Y. R. *Surf. Sci.* **1988**, *200*, L445.
- Superfine, R.; Huang, J. Y.; Shen, Y. R. *Chem. Phys.* **1990**, *172*, 303.
- Baldelli, S.; Mailhot, G.; Ross, P. N.; Shen, Y. R. *J. Phys. Chem. B* **2001**, *105*, 654.
- Baldelli, S. *J. Phys. Chem. B* **2003**, *107*, 6148.
- Baldelli, S.; Markovic, N.; Ross, P. N.; Shen, Y. R.; Somorjai, G. A. *J. Phys. Chem. B* **1999**, *103*, 8920.
- Duffy, D. C.; Davies, P. B.; Bain, D. C. *J. Phys. Chem.* **1995**, *99*, 15241.
- Ward, R. N.; Duffy, D. C.; Davies, P. B.; Bain, C. D. *J. Phys. Chem.* **1994**, *98*, 8536.
- Ward, R. N.; Davies, P. B.; Bain, C. D. *J. Phys. Chem.* **1993**, *97*, 7141.
- Florsheimer, M.; B, M.; Brillert, C.; Wierschem, M.; Fuchs, H. *J. Vac. Sci. Technol. B* **1997**, *15*, 1564.
- Colorado, R. J.; Villazana, R. J.; Lee, T. R. *Langmuir* **1998**, *14*, 6337.
- Wenzl, I.; Yam, C. M.; Barriet, D.; Lee, T. R. *Langmuir* **2003**, *19*, 10217.
- Lee, S.; Puck, A.; Graupe, M.; Colorado, R.; Shon, Y.-S.; Lee, T. R.; Perry, S. S. *Langmuir* **2001**, *17*, 7364.
- Barriet, D., University of Houston, 2005.
- Graupe, M.; Koini, T.; Wang, V. Y.; Nassif, G. M.; Colorado, R. J.; Villazana, R. J.; Dong, H.; Miura, Y. F.; Shmakova, O. E.; Lee, T. R. *J. Fluorine Chem.* **1999**, *93*, 107.
- Lee, T.-C.; Hounihan, D. J.; Colorado, R. J.; Park, J.-S.; Lee, T. R. *J. Phys. Chem. B* **2004**, *108*, 2648.
- Wilbur, J. L.; Biebuyck, H. A.; McDonald, J. C.; Whitesides, G. M. *Langmuir* **1995**, *11*, 825.
- Daniels, M. *Spectrum Extractor for Image J Program*, 1.3.1 ed.; NIH: WI, 2004.
- MacPhail, R. A.; Strauss, H. L.; Snyder, R. G.; Elliger, C. A. *J. Phys. Chem.* **1984**, *88*, 334.
- Snyder, R. G. *J. Chem. Phys.* **1965**, *42*, 1744.
- Snyder, R. G.; Strauss, H. L.; Elliger, C. A. *J. Phys. Chem.* **1982**, *86*, 5145.
- Colthup, N. B.; Daly, L. H.; Wilberley, S. E. *Introduction to Infrared and Raman Spectroscopy*, 3rd ed.; American Press: San Diego, CA, 1990.
- Ong, T. H.; Davies, P. B.; Bain, C. D. *Langmuir* **1993**, *9*, 1836.
- Weinstein, R. D.; Moriarty, J.; Cushnie, E.; Colorado, R. J.; Lee, T. R.; Patel, M.; Alesi, W. R.; Jennings, G. K. *J. Phys. Chem. B* **2003**, *107*, 11626.

JP804707W